Structural modeling of a historic castle using Close Range Photogrammetry

V. Barrile, G. Bilotta, E. D'Amore, G. M. Meduri, S. Trovato

Abstract— This paper presents a methodology for building surveying and structural modeling of buildings of monumental interest. The complex geometry of these structures requires appropriate techniques to support the diagnosis, health monitoring and structural analysis phases for the validation of the expected performance under future earthquakes. This study aims to investigate a low-cost technology to generate accurate 3D structural model of large historical buildings using photos taken by handheld digital cameras and commercial software. In this regard, a multidisciplinary approach, that integrates close-range digital photogrammetry and finite element analysis (FEM), is tested to the case study of a XV-XVI century masonry castle in southern Italy (Marina di Gioiosa Jonica, Reggio Calabria). Furthermore, to assess the accuracy of the modeling process the geometry of the generated model, we compared it against classical buildings surveying techniques. Finally, a linear FEM analysis is undertaken using the 3D model to show the potential of the adopted procedure for the purpose of structural analysis of a complex structure under earthquake loads.

Keywords— Building surveying, Cultural heritage, Earthquake analysis, Historical buildings, Masonry structures, Structural models.

I. INTRODUCTION

CULTURAL heritage requires the implementation of suitable survey techniques for preservation and promotion purposes [1]–[2]–[3].

The introduction of new measuring devices such as 3D laser scanners, spherical photogrammetry, structure-from-motion photogrammetry and the latest methods of image-based modeling produced a strong change in the acquisition, treatment and restitution of metric information. These new techniques allow for the construction of digital photo-realistic 3D models of complex buildings and structures hardly suitable for traditional surveying techniques [4]–[5]–[6]. Models so

V. Barrile is with the DICEAM Department, Faculty of Engineering Mediterranean University of Reggio Calabria, Reggio Calabria 89100 IT (phone: +39-0965-169-2301; e-mail: vincenzo.barrile@unirc.it).

G. Bilotta was with the Department of Planning, IUAV University of Venice, Venice 30135 IT. She now collaborates with the DICEAM Department, Faculty of Engineering Mediterranean University of Reggio Calabria, Reggio Calabria 89100 IT (e-mail: giuliana.bilotta@iuav.it).

E. D'Amore is with the DICEAM Department, Faculty of Engineering Mediterranean University of Reggio Calabria, Reggio Calabria 89100 IT (email: enzo.damore@unirc.it).

G. M. Meduri is with the DICEAM Department, Faculty of Engineering Mediterranean University of Reggio Calabria, Reggio Calabria 89100 IT (email: ing.giuseppemariameduri@gmail.com).

S. Trovato is with the DICEAM Department, Faculty of Engineering Mediterranean University of Reggio Calabria, Reggio Calabria 89100 IT (email: sandro.trovato@unirc.it).

obtained can be integrated in a novel information system capable to manage complex and typologically heterogeneous data relevant for the monitoring and preservation of cultural heritage [7]–[8]. To this purpose, in this paper, promising close-range digital photogrammetric techniques are applied to the case study of Torre Galea, shown in Fig. 1, a relevant Italian XV-XVI century masonry castle built in Marina di Gioiosa Ionica, Reggio Calabria.

The proposed procedure aims at the implementation of the already mentioned digital photogrammetric techniques for the semiautomated generation of an accurate 3D model. The generated model is then converted into a finite element model for the analysis of building performance under static and dynamic loads and for structural health monitoring purposes [9]–[10]–[11]–[12]. Furthermore, to assess the accuracy of the modeling process, we compared the geometry of the generated model against classical buildings surveying techniques.

The first phase of the proposed procedure, digital a stand-alone software (Photoscan by Agisoft) that performs photogrammetric processing of digital images and generates 3D spatial data processes photos of the castle, taken by a handheld

Fig. 1 Views of Torre Galea- Marina di Gioiosa Jonica (RC)

digital camera. Then, for eliminating mesh defects, the generated 3D model is imported into Geomagic Studio software. This software allows for the editing of the point cloud and the mesh. Geomagic also provides advanced surfacing editing functions (e.g. decimation), in addition to accurate functions of 3D data processing.

Finally, we imported the amended model into a FEM software (SAP2000 Rel.17). Linear static and dynamic analyses are performed to investigate the behavior of the structure under gravitational and earthquake loads.

The flow chart of Fig.2 shows the algorithm that, starting from the digital images, yields to the 3D structural model.

II. CONSTRUCTION OF 3D MODEL

The procedure of photographs processing and 3D model construction comprises four main steps as described by Photoscan developers.
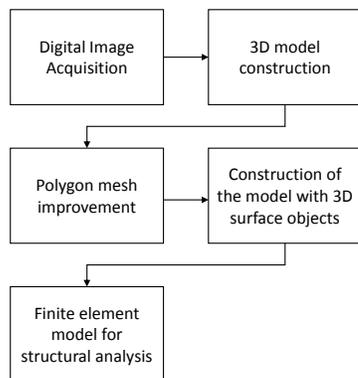
Fig. 2 Algorithm of the adopted procedure for the generation of a 3D structural model from a close-range digital photogrammetric survey.

1. The First step is the camera alignment phase. At this step, PhotoScan seeks common points on the photographs to be

merged. The result of this step is a cloud of sparse points (Fig.3) and a series of camera positions. The point clouds represents the alignment results between photos and will not be used directly in a further procedure of construction of the 3D model. However, it can be exported for further use in external programs. The construction of the 3D model by PhotoScan is based, instead, on the set of data related to camera positions.

2. The next phase is the construction of dense point cloud (Fig.4). Based on the estimated positions of the camera, PhotoScan generates a point cloud more dense and detailed. This point cloud can be modified and classified before being exported with the generation of a three-dimensional mesh model.

3. Then we proceed with the construction of the mesh (Fig.5). PhotoScan reconstructs the surface of a 3D polygon mesh representing the object based on the dense point clouds obtained from the previous step (Fig.6). Generally, there are two algorithmic methods available in PhotoScan that can be applied for the generation of 3D meshes: Field Height - for planar surfaces, or Arbitrary - for any object type.

4. After building the polygonal network, it may be necessary to make some adjustments. PhotoScan is able to make corrections, such as decimation of the mesh, the removal of isolated components, the closing of holes, etc. When a more complex and detailed editing is pursued, an external editing software can be used. In this regard, PhotoScan allows the export of the mesh for further editing with other software. Then, the refined model can be inported in PhotoScan through the most common interchange formats.

5. After the geometry and the mesh has been reconstructed, it can be textured (Fig.7) and/or used for the production of orthophotos. PhotoScan implements several texturing algorithms, described in detail by the software developers.
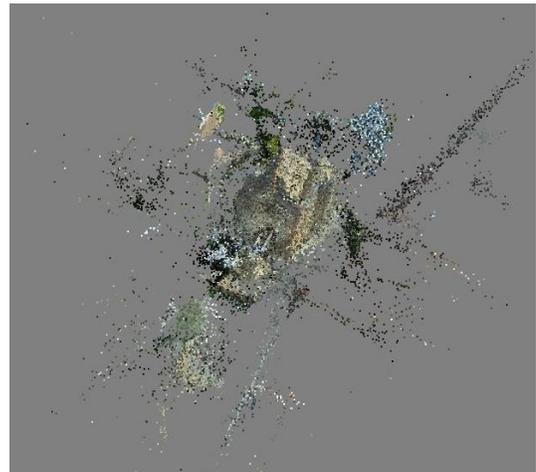
Fig. 3 Point Clouds

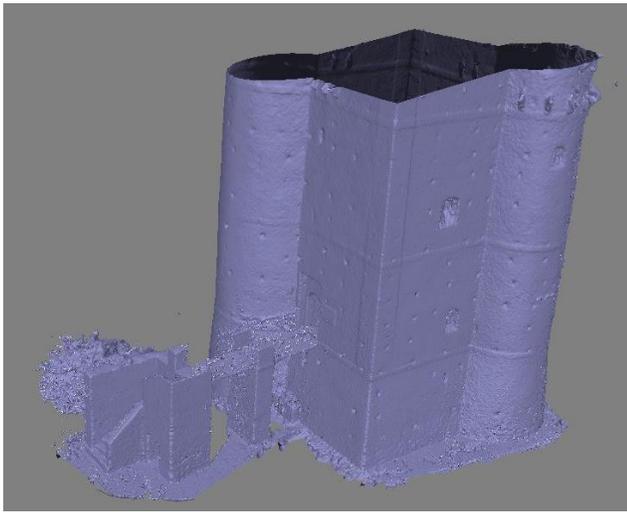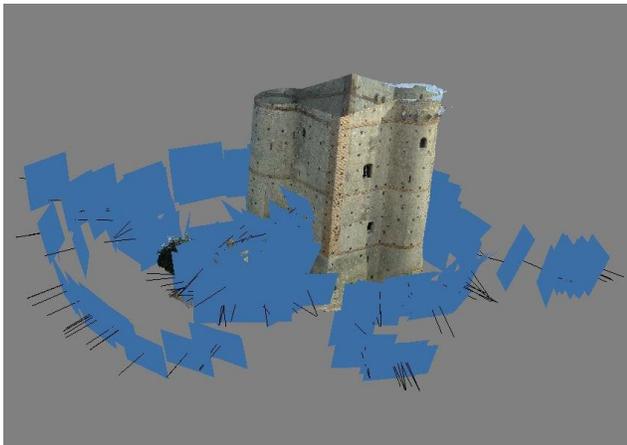Fig. 4 Dense Point Clouds

Fig. 5 Mesh

Fig. 6 Texture with the position of the camera (blue square)

Fig. 7 3D model with texture

We now scaled the obtained 3D model. For the scaling process to be successful, a precise measuring base has to be determined. In our case study, we selected the span of the castle gate as a reference basis.

In order to scale the model we define two markers (Fig.8) that allow for the measurement of the distance between two known points. Then we proceed to create a "scale-bar" and to change the known distance.

Fig. 8 Markers with flags

From the 3D scaled model, we want to move to the FEM software for the structural analysis. This step is not directly possible because the exported mesh is affected by errors related to discrepancy between the various points constituting the mesh; for this reason we cannot import directly into a software FEM the 3d model. We must make an intermediate step to eliminate the defects of the mesh.

We can export the 3D model in different interchange formats. In this work, we used the STL format (Stereo Lithography interface format or Standard Triangulation Language).

III.　POLYGON MESH IMPROVEMENT

For eliminating defects of mesh, we proceed exporting the 3D model from PhotoScan in STL format, and then imported the model into Geomagic Studio software. This software allows for the editing of the point-clouds, of the generated mesh and provides, editing functions of advanced surfacing, in addition to its accurate functions of processing 3D data.

The Mesh Doctor is an automatic improvement of polygon mesh. It is generally recommended to use the Mesh Doctor after importing a polygonal model.

The steps to follow in order to improve the mesh are:

1. Import the model (STL) within Geomagic Studio and set the unit of measurement.

2. The software automatically recognizes the presence of mesh and asks if you want to launch an analysis mesh doctor. The mesh affected by errors are identified directly on the model with red areas (Fig.9).

3. If necessary, we can rescale the model using the specific tool available in Geomagic (Fig.10).

4. The last step is exporting in dxf format for CAD editing.

From here, we create a file that we imported into AutoCAD, from which we have to create a new layer and transfer the imported model on it. Our goal is to build 3Dface objects that are geometric elements that can be imported into SAP2000 or other FEM software. Geomagic software automatically exports 3Dface, the only problem is that it automatically creates a layer named "layer 0". Sap2000 unfortunately requires the use of a different layer that can be created using a CAD software.
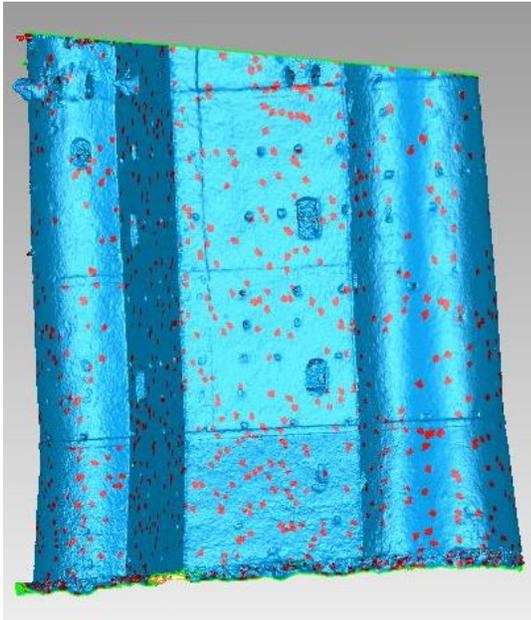

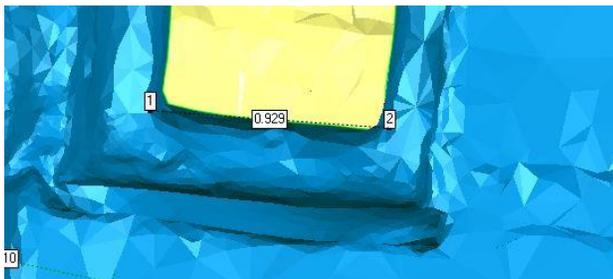Fig. 9 Mesh with damaged areas identified in red

Fig. 10 Measurement of the main entrance by two points in Photoscan

IV. VALIDATION OF THE RESULTS OBTAINED WITH THE PHOTOGRAMMETRIC SURVEY

3D photogrammetry is affected by inherent errors [13]–[14] arising from processing algorithms and by those typical of photography.

Picture quality, for instance, is limited by sensor resolution, lens optical deformation and picture prospective. The latter requiring straightening of the image with consequent dimensional and parallax errors.

Other well-known error source arise from image mosaicking [15]. To assess the accuracy of the model, a set of repeated measurements were taken on selected part of the building to be compared with reference measurement taken with precision

instruments (TOPCON Electronic Total Station, GTS-312).

The need to perform multiple measurements on the 3D model derives from the uncertainty offered by the pointing system for the measurements inside the photogrammetric software.

The results of the comparisons for some of the elements of the building (see Figs.10-11), along with the errors in term of difference and percentage difference are given in Tables 1-8.

Finally, Table 9 shows the mean and standard deviation on the measured element of the structure.

We can note that error between the measurements obtained with the survey and the 3D model obtained from Photoscan, after the scaling, is always less than 1%.
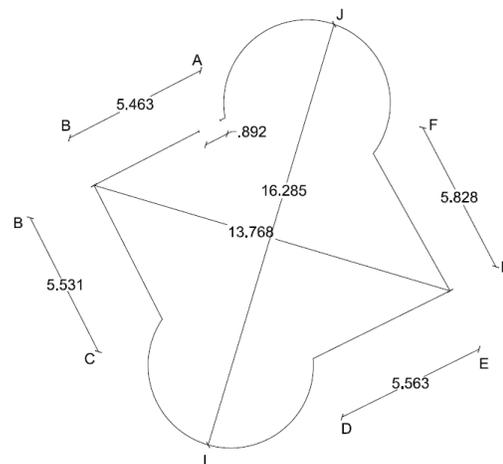

Fig. 11 Measurement from Photoscan

Fig. 12 Planimetric survey and measured elements (TOPCON Electronic Total Station, GTS-312)
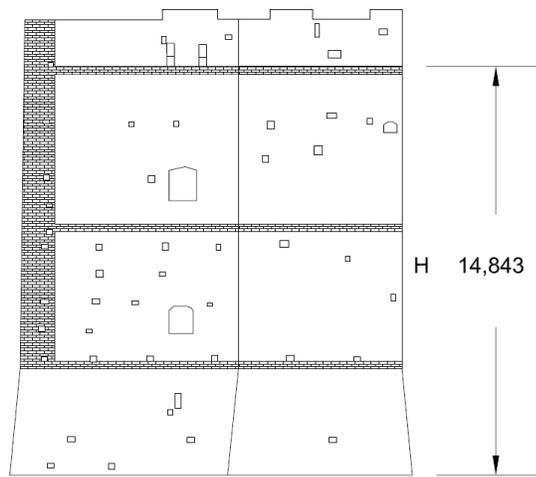
Fig. 13 Perspective drawing

Table 1. Comparison between survey and Photoscan measurements – AB element

n	Survey [m]	Photoscan [m]	Δ [m]	Δ%
1	5,463	5,435	0,0282	0,52%
2	5,463	5,429	0,0343	0,63%
3	5,463	5,496	-0,0332	-0,61%
4	5,463	5,434	0,0290	0,53%
5	5,463	5,501	-0,0383	-0,70%
6	5,463	5,431	0,0315	0,58%

Table 2. Comparison between survey and Photoscan measurements – BC element

n	Survey [m]	Photoscan [m]	Δ [m]	Δ%
1	5,531	5,564	-0,0324	-0,59%
2	5,531	5,496	-0,0351	-0,64%
3	5,531	5,555	0,0234	0,42%
4	5,531	5,502	0,0290	0,52%
5	5,531	5,563	-0,0313	-0,57%
6	5,531	5,494	0,0375	0,68%

Table 3. Comparison between survey and Photoscan measurements – CD element

n	Survey [m]	Photoscan [m]	Δ [m]	Δ%
1	5,563	5,598	-0,0345	-0,62%
2	5,563	5,534	0,0289	0,52%
3	5,563	5,533	0,0299	0,54%
4	5,563	5,592	-0,0290	-0,52%
5	5,563	5,595	-0,0321	-0,58%
6	5,563	5,526	0,0367	0,66%

Table 4. Comparison between survey and Photoscan measurements – EF element

n	Survey [m]	Photoscan [m]	Δ [m]	Δ%
1	5,829	5,801	0,0279	0,48%
2	5,829	5,795	0,0335	0,57%
3	5,829	5,858	-0,0295	-0,51%
4	5,829	5,862	-0,0336	-0,58%
5	5,829	5,804	0,0250	0,43%
6	5,829	5,794	0,0344	0,59%

Table 5. Comparison between survey and Photoscan measurements – BE element

n	Survey [m]	Photoscan [m]	Δ [m]	Δ%
1	13,768	13,713	0,0555	0,40%
2	13,768	13,830	-0,0615	-0,45%
3	13,768	13,834	-0,0653	-0,47%
4	13,768	13,710	0,0585	0,42%
5	13,768	13,715	0,0529	0,38%
6	13,768	13,700	0,0682	0,50%

Table 6. Comparison between survey and Photoscan measurements – IJ element

n	Survey [m]	Photoscan [m]	Δ [m]	Δ%
1	16,285	16,344	-0,0588	-0,36%
2	16,285	16,350	-0,0651	-0,40%
3	16,285	16,237	0,0477	0,29%
4	16,285	16,342	-0,0568	-0,35%
5	16,285	16,213	0,0716	0,44%
6	16,285	16,216	0,0686	0,42%

Table 7. Comparison between survey and Photoscan measurements – H element

n	Survey [m]	Photoscan [m]	Δ [m]	Δ%
1	14,843	14,777	0,0665	0,45%
2	14,843	14,902	-0,0593	-0,40%
3	14,843	14,913	-0,0782	-0,53%
4	14,843	14,765	0,0699	0,47%
5	14,843	14,768	0,0747	0,50%
6	14,843	14,922	-0,0786	-0,53%

Table 8. Comparison between survey and Photoscan measurements – Main entrance

n	Survey [m]	Photoscan [m]	Δ [m]	Δ%
1	0,892	0,886	0,0064	0,72%
2	0,892	0,883	0,0087	0,97%
3	0,892	0,885	0,0072	0,81%
4	0,892	0,898	-0,0056	-0,63%
5	0,892	0,897	-0,0048	-0,53%
6	0,892	0,885	0,0073	0,82%

Table 9. Mean value μ and deviation σ of the measurements

Element	μ [m]	σ [m]
A-B	0,0086	0,0314
B-C	0,0024	0,0317
D-E	0,0000	0,0320
E-F	0,0096	0,0293
B-E	0,0180	0,0578
I-J	0,0012	0,0620
H	0,0019	0,0715
Main entrance	0,0032	0,0060

V. STRUCTURAL ANALYSIS

At this stage, the model of the castle is first imported into AutoCAD to be rearranged.

Then the model is exported in Drawing Exchange Format (DXF).

DXF entities should be organized by assigning to a different layer each DXF entity to matching objects of the finite element analysis software.

The finite element software Sap2000 (SAP2000 CSI inc. Berkeley, Cal, US) was selected for the analysis and the correspondence-table between DXF entities and Sap2000 objects are shown in Table 10.

DXF files are finally imported into SAP2000 using the software specific import procedure.

Table 10. DXF entities - SAP2000 objects correspondence table

DXF entity	SAP2000 object	Color
Point	Joint	Yellow
Line	Frame	Yellow
Point	Link (one-point)	Green
Line	Link (two-point)	Green
3D Face	Shell	Red
Polygon Mesh	Solid	White

A snapshot of the finite element model after the import procedure in SAP2000 is given in Fig.14 with some properties (number of degrees of freedom, number of dynamic degrees of freedom and number of triangular shells) included in Table 11.

Table 11. Properties of the imported SAP2000 model

Number of degrees of freedom	395.682
Number of mass degrees of freedom	197.841
Number of shell elements	145.352

For the assessment of the finite element model generated by the proposed procedure the structural analysis under seismic design load is performed.

It should be noted that an accurate structural analysis would require the estimation of the mechanical properties of the materials through experimental tests [16]–[17]. However, for the purpose of this preliminary analysis phase, mechanical properties suggested by the Italian building code for similar masonry typologies [18] are assigned to shell elements (see Table 12). Thickness of masonry walls varies from 2.5 m at the base to a minimum of 1.5m at the roof. The software automatically calculates the total mass of the structure, equal to 2396 t.

Table 12. Mechanical properties of masonry elements

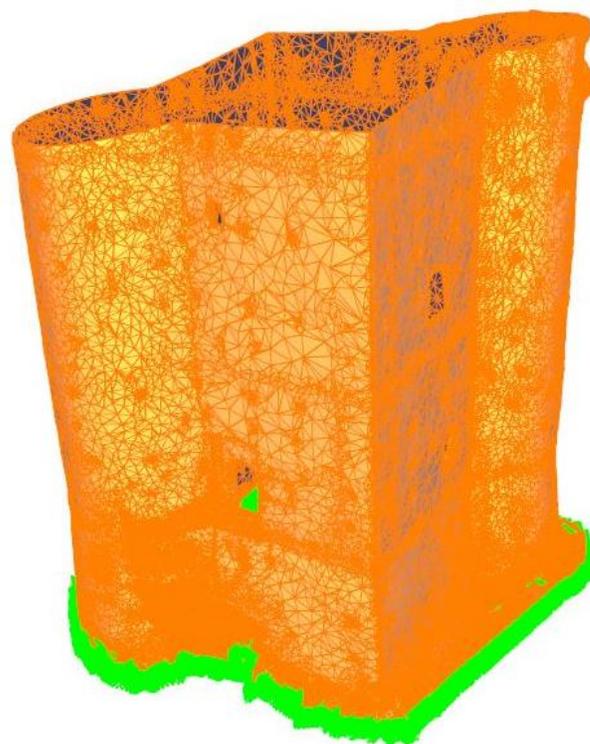| Type of stone masonry	f_m $\left(N/cm^2\right)$	τ_0 $\left(N/cm^2\right)$	E $\left(N/mm^2\right)$	G $\left(N/mm^2\right)$	γ $\left(KN/m^3\right)$
Squared Coursed blocks	800	12.0	3200	940	22
f_m= compressive strength, τ_0=shear strength, E=elastic modulus, $G=$ Shear modulus, γ = unit weight					

Fig. 14 Imported model in Sap2000

Seismic analysis to special provision for existing structures of the Italian building code is performed. Site-specific response-spectrum for the considered life-safety limit state is evaluated using parameters included in Table 13 with the resulting elastic response spectrum shown in Fig. 15.
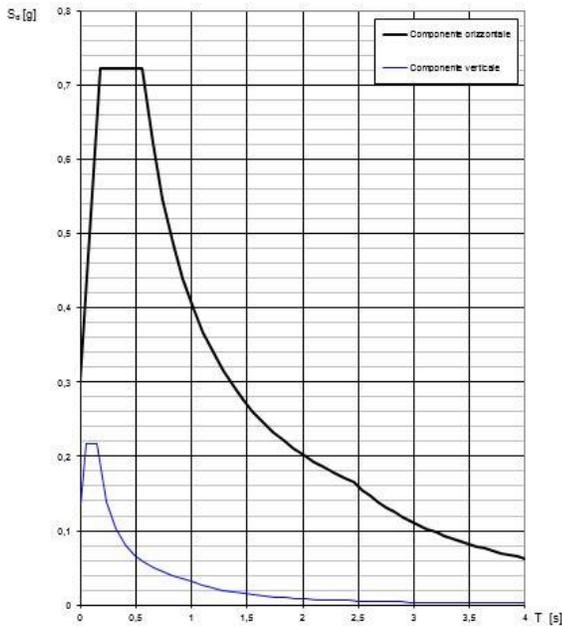
Fig. 15 Elastic response spectrum at the life-safety limit state

Table 13. Design parameters for the evaluation of the acceleration response spectrum.

Nominal life V_N [years]	50
Functional type C_U [-]	III
Design reference life V_R [years]	75

Results of the modal analysis (see Table 14) show that the first (Fig.16) and the second mode (Fig.17) are mainly translational along the weak-axis, i.e. orthogonal to the line connecting the two circular towers, and the strong-axis of the structure, respectively. The third mode (Fig.18) exhibits, instead, a relevant rotational component.

Principal stresses from gravity load analysis are shown in Fig.19. These results show limited and reasonable stress concentration, giving a good feedback on the quality of the finite element model.

Furthermore, compressive stresses at the base of the structure, with values varying between 3.15 daNcm^{-2} and 4.54 daNcm^{-2}, are quite close to the mean vertical stress component at the base, simply obtainable by taking the ratio of the total weight over the structure base area, equal to 3.74 kgcm^{-2}.

Table 14. Mass participation ratio and their summation along the degrees of freedom X, Y and rotational Z for the first 5 modes.

Mode n.	Period (s)	Mass ratio X	Mass ratio Y	Sum Mass ratio X	Sum Mass ratio Y	Mass ratio RZ	Sum Mass ratio RZ
1	0.211	0.203	0.390	0.203	0.390	0.004	0.004
2	0.156	0.238	0.113	0.441	0.502	0.003	0.007
3	0.143	0.029	0.058	0.471	0.560	0.147	0.154
4	0.141	0.157	0.060	0.628	0.620	0.107	0.261
5	0.092	0.000	0.000	0.628	0.620	0.418	0.679

Moreover, an equivalent static analysis is performed combining the seismic input in one direction, i.e. X or Y, with the 30% of the orthogonal one.

Maximum and minimum principal stress components for the shell elements subjecting the model to the mentioned lateral forces are shown in Fig.20. Shear stress values comprised between 1.92 daNcm^{-2} and 2.69 daNcm^{-2}, see Fig.21, show that there are not anomalous stress concentrations due to poor meshing. Other stress components are not included here for brevity.

Finally, a preliminary stress-check under seismic loads is performed here by comparing design stress components at the base of the structure (seismic demand) against shear stress capacity. The design shear capacity V_t is estimated by the following equation [18]:

$$\frac{V_t}{l \cdot t} = \frac{1.5 \cdot \tau_{0d}}{b} \sqrt{1 + \frac{\sigma_0}{1.5 \cdot \tau_{0d}}}, \qquad (1)$$

where

l is the length of the wall;
t is the thickness of the wall;
σ_0 is the vertical mean stress component divided to the confidence factor;
b is a coefficient ($1 \leq b \leq 1.5$) equal to h/l, where h is the height of the wall;
τ_{0d} design shear strength (see Table 12).

Table 15. Demand to Capacity ratio under seismic load at the base of the structure.

τ_0 (daN/cm^2)	$\frac{V_t}{l \cdot t}$ (daN/cm^2)	D/C
1,92 ÷ 2,69	2,95	0,65 ÷ 0,91
τ_0= seismic shear stress component; $\frac{V_t}{l \cdot t}$=design shear capacity; D/C=demand to capacity ratio		

The values of the shear stress τ_0 and vertical stress component σ_0 are given in Table 15. The results of this analysis show a Demand to Capacity ratio varying between 0,65 and 0,91 at the base of the structure which is lower than the limiting value of 2,25 suggested by the Italian code provisions.

Moreover, it appears that at some locations stress concentrations, due to rapid change in mesh geometry, are still noticeable.
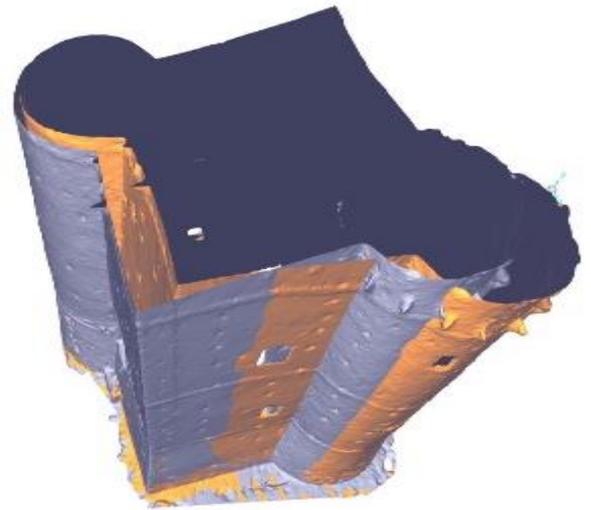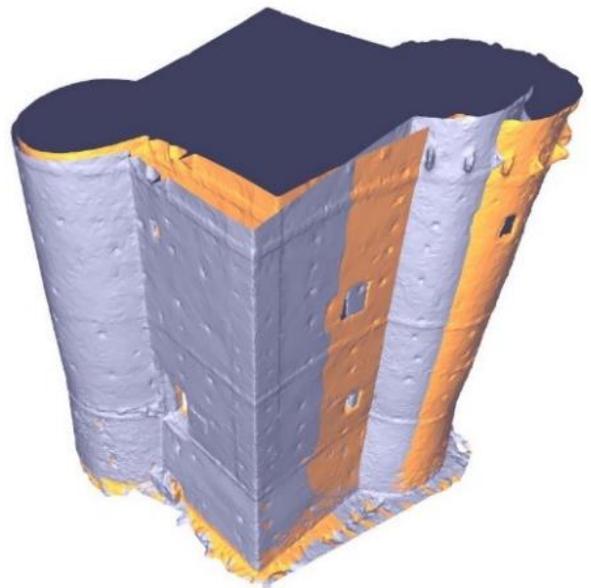
(a)

(a)

(b)
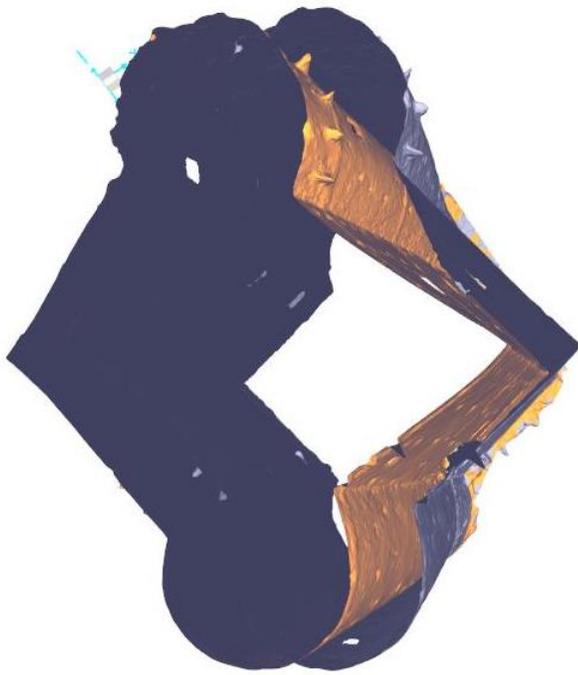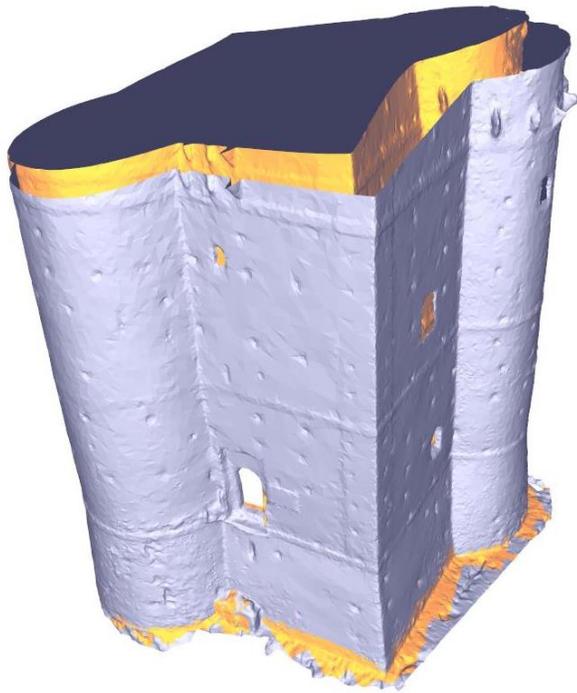
(b)

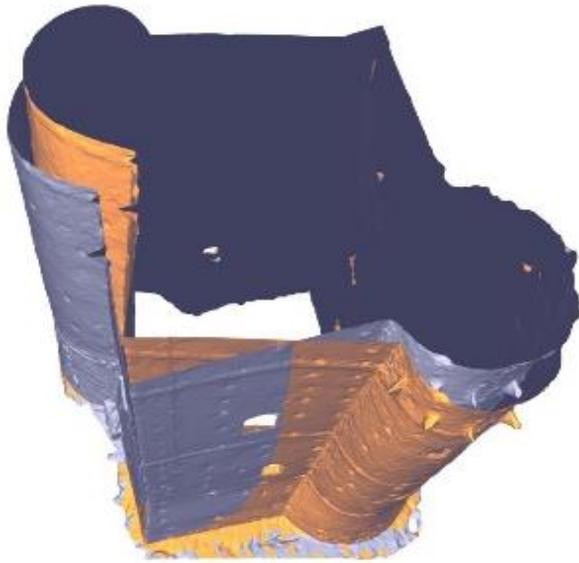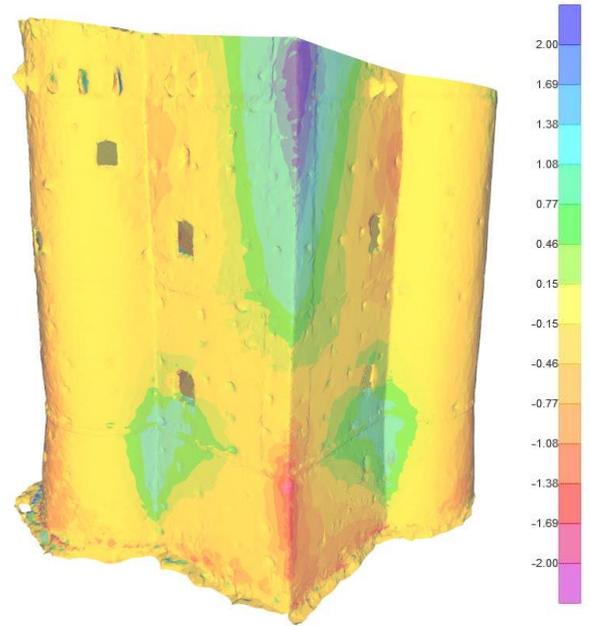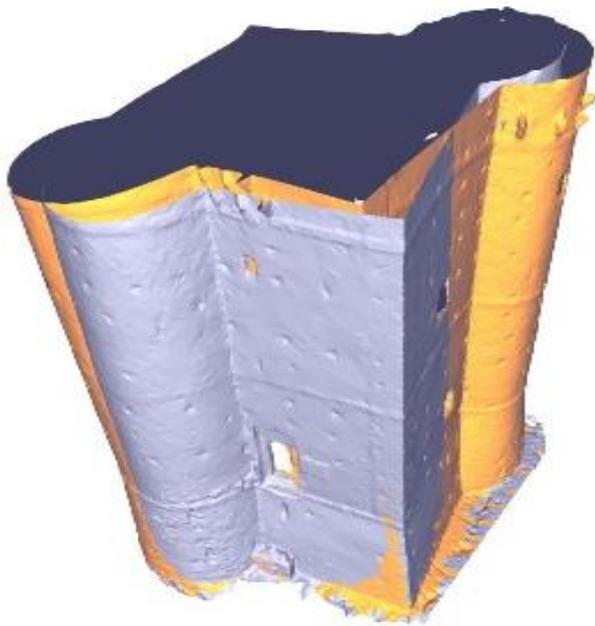Fig. 16 First mode T= 0.211 sec (Grey = undeformed shape): (a) top view and (b) lateral view

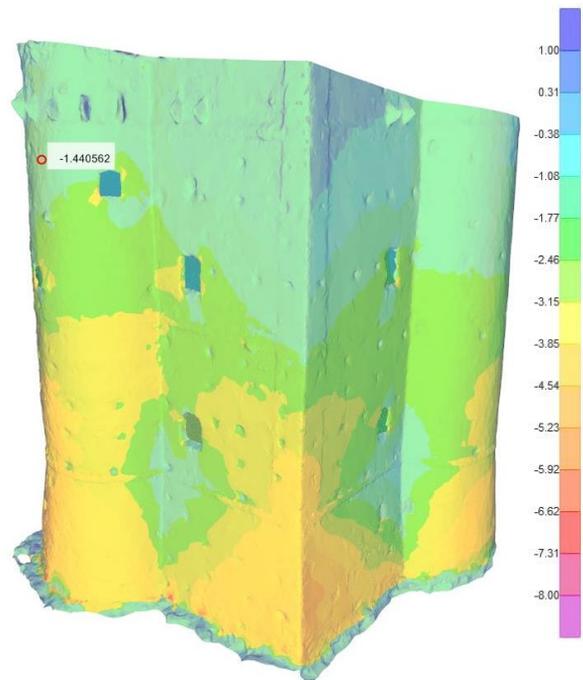Fig. 17 Second mode T= 0.156 sec (Grey = undeformed shape): (a) top view and (b) lateral view

(a)

(a)
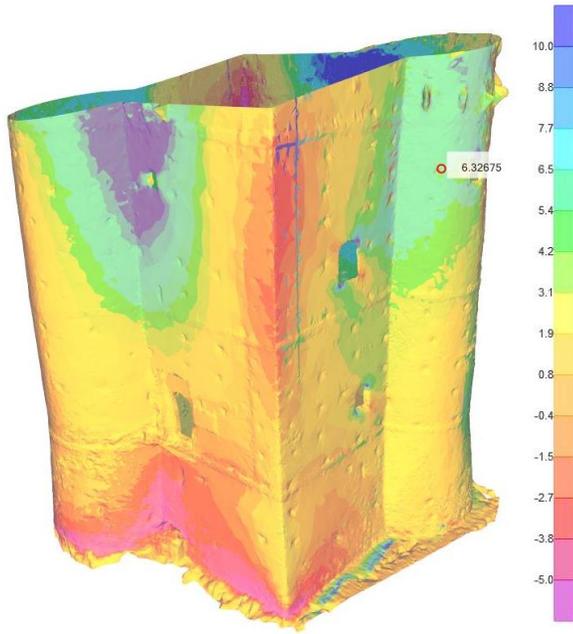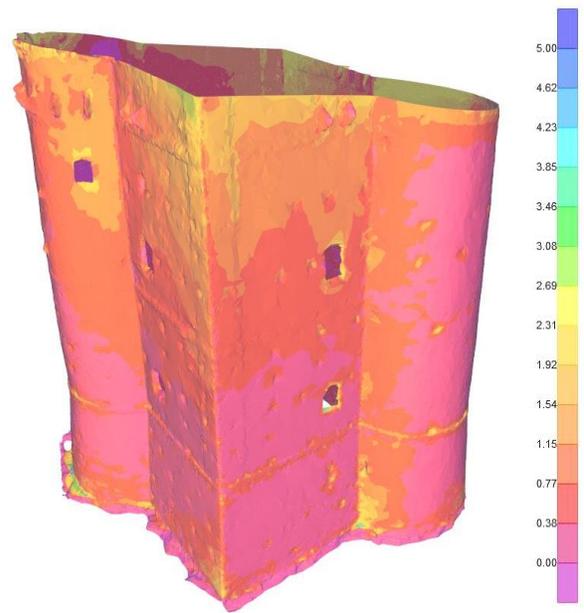

(b)

(b)

Fig. 18 Third mode T= 0.143 sec (Grey = undeformed shape): (a) top view and (b) lateral view
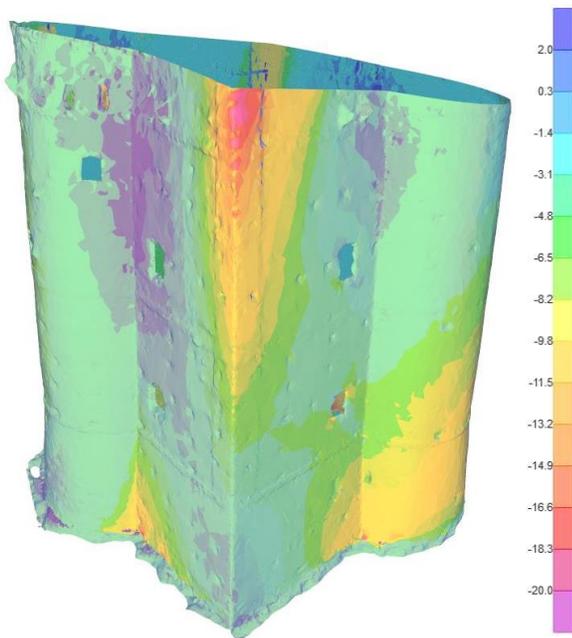
Fig. 19 Minimum (a) and maximum (b) principal stress (kg/cm2) for the gravity load combination
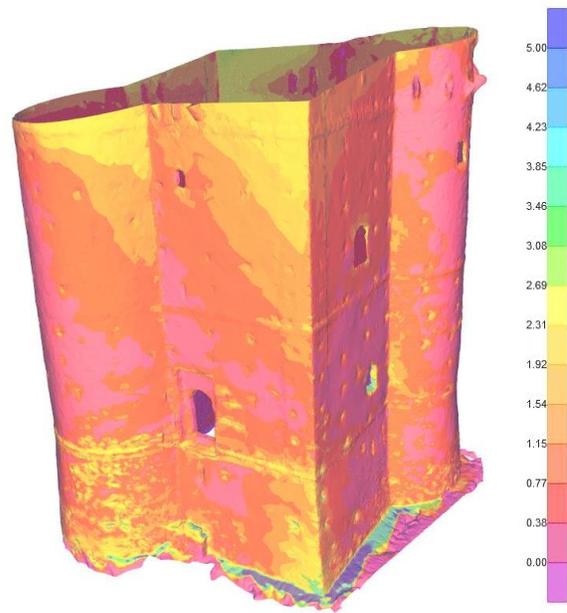
(a)

(a)

(b)

(b)

Fig. 20 Minimum (a) and maximum (b) principal stress (kg/cm²) for the seismic load combination in the *x* direction plus 30% in *y* direction

Fig. 21 Shear stress (kg/cm²) for the seismic load combination in the *x* direction plus 30% in *y* direction

VI. CONCLUDING REMARKS

The techniques used in this work have shown the feasibility of low-cost photogrammetry for survey and structural modeling purposes of a relevant construction. The adopted procedure, even though not completely automated, is capable to produce - contactless and without the need of many known reference points - a satisfactory 3D model from digital images with a degree of accuracy totally beyond the reach of ordinary survey techniques.

However, even though promising, some issues arise from the great number of 3D-faces produced by the automated generation algorithms, requiring further post-processing efforts for the reduction of the finite elements mesh to a more manageable size, and from to the inability to differentiate, during the acquisition phase, the mechanical properties of different part of the model. Furthermore, the generated mesh still needs further refinement to fix various mesh errors.

REFERENCES

[1] A. Bandiera, J.A. Beraldin, M. Gaiani, "Nascita ed utilizzo delle tecniche digitali di 3D imaging, modellazione e visualizzazione per l'architettura e i beni culturali" in *Ikhnos*, 2011, pp 81-134.

[2] G. Guidi, M. Russo, J.A. Beraldin, *Acquisizione 3D e modellazione poligonale,* McGraw-Hill, 2010.

[3] L. Barazzetti, G. Forlani, F. Remondino, R. Roncella, M. Scaioni M "Experience and achievements in automated image sequence orientation for close-range photogrammetric projects" in *Proc. of SPIE Optics+Photonics, 23-26 May*, Munich, Germany, vol. 8085, 2011.

[4] V. Barrile, G.M. Meduri, G. Bilotta, "Comparison between Two Methods for Monitoring Deformation with Laser Scanner", in *WSEAS Transactions on Signal Processing*, vol. 10, 2014, pp. 497-503. ISSN: 1790-5052.

[5] A. Bhatla, S.Y. Choe, O. Fierro, F. Leite, "Evaluation of accuracy of as-built 3D modeling from photos taken by handheld digital cameras.", in *Automation in Construction*, Elsevier BV, vol. 28, pp. 116-127.

[6] V. Barrile, G.M. Meduri, G. Bilotta, "Experimentations and Integrated Applications Laser Scanner/GPS for Automated Surveys", in *WSEAS Transactions on Signal Processing*, vol. 10, 2014, pp. 471-480. ISSN: 1790-5052

[7] V. Barrile, G.M. Meduri, G. Bilotta, "Laser scanner technology for complex surveying structures" in *WSEAS Transactions on Signal Processing*, vol. 7, 2011, pp. 65-74. ISSN: 1790-5052

[8] V. Barrile, G.M. Meduri, G. Bilotta, "Laser scanner surveying techniques aiming to the study and the spreading of recent architectural structures" in *Recent Advances in Signal and Systems, Proceedings of the 9th WSEAS International Conference on Signal, Speech and Image Processing (SSIP '09)*, 2009, pp. 92-95. ISSN: 1790-5109

[9] E. D'Amore, S. Trovato, "Experimental analysis for identification of bridges structural damage Operational using Modal Analysis based methods" in *Proceedings of 15th World Conference on Earthquake Engineering* (15 WCEE), 2012.

[10] A. Carpinteri, G. Lacidogna "Damage Monitoring of an Historical Masonry Building by the Acoustic Emission Technique" in *Materials and Structures*, vol. 39, 2007, pp. 161-167.

[11] I. Lubowiecka , P. Arias, B. Riveiro, M. Solla, "Multidisciplinary approach to the assessment of historic structures based on the case of a masonry bridge in Galicia (Spain)" in *Computers & Structures*, Elsevier Ltd, 89, 2011, pp. 1615-1627.

[12] P. Arias, J. Herráez, H. Lorenzo, C. Ordóñez, "Control of structural problems in cultural heritage monuments using close-range photogrammetry and computer methods" in *Computers & Structures*, vol. 83, 2005, pp. 1754-1766.

[13] X. Li, "Photogrammetric investigation into low-resolution digital camera systems", Thesis (Ph. D.) Dept. of Geodesy and Geomatics Engineering, University of New Brunswick, 1999.

[14] T. Läbe, W. Förstner, "Geometric stability of low-cost digital consumer cameras" in *Proceedings of the 20th ISPRS Congress, Istanbul, Turkey*, 2004, pp. 528-535.

[15] R.B. Inampudi, "Image mosaicking. IGARSS '98. Sensing and Managing the Environment" in *1998 IEEE International Geoscience and Remote Sensing Symposium Proceedings*, vol. 5, 1998, pp. 2363-2365.

[16] L. Rovero, V. Alecci, J. Mechelli, U. Tonietti, M. De Stefano, "Masonry walls with irregular texture of L'Aquila (Italy) seismic area: validation of a method for the evaluation of masonry quality" in *Materials and Structures*, Springer Netherlands, 2015, pp. 1-18.

[17] M. Tomaževič, "Shear resistance of masonry walls and Eurocode 6: shear versus tensile strength of masonry" in *Materials and Structures* vol. 42, 2009, pp. 889-907.

[18] NTC, D.M. del Ministero delle Infrastrutture e dei Trasporti del 14 gennaio 2008. Nuove Norme Tecniche per le Costruzioni, 2008.

Software:
Agisoft PhotoScan v.1.1 (http://www.agisoft.com/).
Autodesk AutoCAD 2016 (http://www.autodesk.it/).
CSI Sap2000 v.17.1 (http://www.csi-italia.eu/).
Geomagic Studio 2013 (http://www.geomagic.com).